Magnetization of armchair carbon tori

C. C. Tsai,[1] F. L. Shyu,[2] C. W. Chiu,[1] C. P. Chang,[3] R. B. Chen,[4] and M. F. Lin[1]
[1]*Department of Physics, National Cheng Kung University, 701 Tainan, Taiwan*
[2]*Department of Physics, Chinese Military Academy, 830 Kaohsiung, Taiwan*
[3]*Center for General Education, Tainan Woman's College of Arts and Technology, 701 Tainan, Taiwan*
[4]*Center for General Education, National Kaohsiung Marine University, 830 Kaohsiung, Taiwan*
(Received 16 January 2004; revised manuscript received 14 May 2004; published 26 August 2004)

Magnetoelectronic states of armchair carbon tori are studied by the tight-binding model. They strongly depend on the magnitude and the direction of the magnetic field (**B**). **B** induces the destruction of state degeneracy, the change of energy spacing, and the semiconductor-metal transition (SMT). SMT's happen more frequently when **B** is relatively close to the toroid axis. Such characteristics are directly reflected in magnetic properties. Magnetization (**M**) exhibits special jump structures at $T=0$, mainly owing to SMT's. Magnitude of **M** and magnetism are mainly determined by the toroid radius (R), the temperature, the angle (α) between the magnetic field and the symmetry axis, and the chirality. The dependence of M on radius (temperature) is strong at $\alpha=0°$, but weak at $\alpha=90°$. Most of armchair carbon tori are paramagnetic for $\alpha>30°$. The critical angle in determining magnetism is $\alpha_c \simeq 30°$. Armchair carbon tori quite differ from carbon tori near zigzag configuration (or armchair carbon nanotubes) in magnetoelectronic structures and magnetism.

DOI: 10.1103/PhysRevB.70.075411 PACS number(s): 73.20.At, 75.10.−b, 71.15.Ap

I. INTRODUCTION

Carbon atoms can form many kinds of system, such as diamond, graphite, straight carbon nanotube (SCN's), and toroidal carbon nanotubes (or carbon tori). SCN's were discovered in 1991 by Iijima.[1] Each SCN is a rolled-up graphite sheet in the hollow cylindrical structure. When the open two ends of a SCN knits together, a carbon toroid could be formed. This quasi-zero-dimensional toroidal system was recently found by Liu *et al.*[2] A carbon toroid is rolled from the origin of a graphite sheet to the two vectors $\mathbf{R_x}=m\mathbf{a}_1+n\mathbf{a}_2$ and $\mathbf{R_y}=p\mathbf{a}_1+q\mathbf{a}_2$, simultaneously.[3] $\mathbf{a}_1$ and $\mathbf{a}_2$ are the primitive lattice vectors of a graphite sheet. The parameters (m,n,p,q) uniquely define the geometric structure. This work is mainly focused on armchair carbon tori with armchair structures along the transverse direction ($\hat{\mathbf{R}}_\mathbf{x}=\hat{x}$) and zigzag structures along the longitudinal direction ($\hat{\mathbf{R}}_\mathbf{y}=\hat{y}$). A $(m,m,p,-p)$ armchair carbon toroid has radius and height $R=\sqrt{3}pb/2\pi$ and $2r=3mb/\pi$, respectively. $b=1.42$ Å is the C-C bond length. Other carbon tori are also taken into account for a complete study. Geometric structures determine whether a carbon toroid is metallic or semiconducting. The main features of the magnetoelectronic structures would be directly reflected in other physical properties, such as magnetic properties and optical excitations.

Carbon tori have attracted a lot of studies on geometric structures,[3–8] electronic structures,[3,6–12] magnetic properties,[12–18] electronic excitations,[18–20] optical properties,[21,22] thermal properties,[23] and transport properties.[24,25] The tight-binding model has been used to obtain the π-electron states.[3,6–18] The dependence on the geometric structures is strong. When a carbon toroid exists in a $\mathbf{B}_\parallel$ field parallel to the symmetry axis, electronics states can exhibit the periodic Aharonov-Bohm oscillations in the absence of the Zeeman effect.[10–12] The closely related system, SCN's, had also been investigated for their electronic structures at any magnetic field.[26–35] The direction of magnetic field significantly affects electronic structures, such as, energy dispersion, state degeneracy, and energy gap. It is expected to play an important role on magnetoelectronic states of carbon tori.

When carbon tori are threaded by the magnetic flux ϕ, the longitudinal angular momentum would change from L to $L+\phi/\phi_0(\phi_0=hc/e)$. The previous studies show that magnetization (**M**) is a periodic function of ϕ with a period ϕ_0, and it is antisymmetric about $\phi_0/2$.[12–18] Whether carbon tori are paramagnetic or diamagnetic is dominated by radius, height, and chirality. There are several studies on magnetic properties of SCN's.[27,28,36] For $\mathbf{B}_\parallel$, the $2m+n=3I$ SCN's (I an integer) are paramagnetic, and the others (the large-gap SCN's) are diamagnetic. On the other hand, all SCN's are diamagnetic in the presence of the perpendicular magnetic field ($\mathbf{B}_\perp$). The main effects of the field direction on magnetic properties of carbon tori would be studied in detail, e.g., the dependence of the magnetism on the field direction. The important differences between armchair carbon tori (zero-dimensional carbon tori) and nonarmchair carbon tori (one-dimensional carbon nanotubes) are also investigated. We hope that such a study is useful in the full understanding of the magnetic properties of the carbon-related nanosystems.

In this work, we mainly study magnetoelectronic structures and magnetic properties of armchair carbon tori. The tight-binding model is used to calculate state energy, energy gap, density of state (DOS), and magnetization. Magnetoelectronic properties are very sensitive to the changes in the radius, the chirality, the temperature, the Zeeman splitting, and the direction and the magnitude of **B**. Comparison with nonarmchair carbon tori or armchair carbon nanotubes is made.

This paper is organized as follows. In Sec. II, the π-electronic states from the $2p_z$ orbitals are calculated for

any magnetic field. Magnetoelectronic states and magnetization are discussed in Sec. III. Finally, Sec. IV contains the concluding remarks.

II. MAGNETOELECTRONIC PROPERTIES WITHIN THE TIGHT-BINDING MODEL

We first see electronic states of an armchair $(m,m,p,-p)$ carbon toroid in the absence of magnetic field. The π-electronic states due to the $2p_z$ orbitals are obtained from the nearest-neighbor tight-binding model. They are derived from those of a graphite sheet, but with the periodical boundary conditions along the transverse $(\hat{x})$ and the longitudinal $(\hat{y})$ directions taken into account. The discrete energy states are characterized by the transverse $(J=k_x r=1,2,3,\ldots,2m)$ and the longitudinal $(L=k_y R=1,2,\ldots,p)$ angular momenta. The curvature effect, the misorientation of the $2p_z$ orbital on the cylindrical surface, is also included in the calculations. It will affect the nearest-neighbor interactions; that is, $\gamma's$ might be different along the longitudinal and the transverse directions: $\gamma_1=\gamma_0(1-b^2/32r^2)$, $\gamma_2=\gamma_0(1-b^2/8r^2)$; $\gamma_3=\gamma_1$.[37,3] $\gamma_0(\sim 3\ \mathrm{eV})$[11,12] is the nearest-neighbor interaction of A atom and B atom.

An armchair carbon toroid exists in a uniform magnetic field $\mathbf{B}$. There is an angle (α) between $\mathbf{B}$ and the toroidal axis $(\hat{z})$, i.e., $\mathbf{B}=\mathbf{B}\cos\alpha\hat{\mathbf{z}}+\mathbf{B}\sin\alpha\hat{\mathbf{R}}=\mathbf{B}_{\parallel}+\mathbf{B}_{\perp}$. It is convenient in using the cylindrical coordinates (R,Φ,z) $(\hat{y}\|\hat{\Phi};\ \Phi=y/R)$. The vector potential is chosen to be $\mathbf{A}=RB\cos\alpha/2\hat{\Phi}+RB\sin\alpha\sin\Phi\hat{z}$. It causes the magnetic phase factor $G=\int\mathbf{A}\cdot d\mathbf{R}$.[38] Consequently the former and the latter, respectively, lead to the shift of L $(L\rightarrow L+\cos\alpha\phi/\phi_0;\ \phi=\pi R^2 B)$ and the coupling of different L's. Such coupling would make calculations become very complicated, since it affects the quantization of wave function. When the magnetic field is absent, each state is described by an independent L. Wave function in the presence of $\mathbf{B}$ is the linear combination of the tight-binding functions of different $L's$. The coupling effect of angular momentum J can be neglected because of $R\gg 10r$. The Hamiltonian matrix is built from the space spanned by the different $L's$. The nearest-neighbor Hamiltonian matrix element associated with A atom and B atom is[34]

$$H_{L'L}^{BA}=-\frac{1}{2pm}\times\sum_{R_A,R_B}\gamma_j e^{-i(L'-L)/Ry}e^{-iJ(x'-x)r}e^{-i\left(L'+\frac{\phi}{\phi_0}\cos\alpha\right)/R(y'-y)}e^{i\Delta G},\tag{1}$$

where the phase difference due to the perpendicular magnetic field is

$$\Delta G=\begin{cases}\dfrac{2\phi\sin\alpha(x'-x)}{\phi_0(y'-y)}\left[\cos\left(\dfrac{y}{R}\right)-\cos\left(\dfrac{y'}{R}\right)\right] & \text{if } \Delta y\neq 0,\\ \dfrac{2\phi\sin\alpha(x'-x)}{\phi_0 R}\sin\left(\dfrac{y}{R}\right) & \text{if } \Delta y=0.\end{cases}\tag{2}$$

The positions of carbon atoms are $\mathbf{R_A}=(x,y)$ and $\mathbf{R_B}=(x',y')$. Equation (1) can be further generalized to the nonarmchair carbon tori. It is relatively complex for chiral carbon tori. State energy $E^h(J,L,\phi)$ can be obtained from the diagonalization of the $2p\times 2p$ Hamiltonian matrix. $h=v\ (c)$ represents the $\pi\ (\pi^*)$ state, with $E^v(J,L,\phi)<0[E^c(J,L,\phi)>0]$. The Zeeman splitting energy $E_z(\sigma,\phi)=\frac{g\sigma}{\mu^* R^2}\frac{\phi}{\phi_0}$. $g\approx 2$, $\sigma=\pm 1/2$ is the electron spin, and μ^* is the bare electron mass. The total energy is $E^h(J,L,\phi;\sigma)=E^h(J,L,\phi)+E_z(\sigma,\phi)$. There might be an energy gap (E_g) between the highest occupied states (HOS) and the lowest unoccupied states (LUS) for a semiconducting carbon toroid. But for a metallic carbon torus, both HOS and LUS are just located at the Fermi level $(E_F=0)$. Density of states is useful in further understanding the low energy electronic structures. It is defined as

$$D(\omega,\phi)=\sum_{h,J,L,\sigma}\frac{1}{\pi}\frac{\Gamma}{[E^h(J,L,\phi;\sigma)-\omega]^2+\Gamma^2},\tag{3}$$

$\Gamma=5\times 10^{-5}\ \gamma_0$ is the broadening parameter.

Although carbon tori are closely related to SCN's in geometric and electronic structures, there are certain important differences in magnetoelectronic properties. The parallel and perpendicular magnetic fields in SCN's, respectively, result in the shift of the transverse angular momentum J and the coupling of the different J's. The changes of state energies in carbon tori are less obvious, as compared with those in SCN's. For example, the magnetic field hardly affects the large-gap carbon tori with $2m+n\neq 3I$ (neglected in this work; I an integer), while it could induce the semiconductor-metal transition (SMT) in the large-gap carbon nanotubes.[26] As a result, these two systems would behave very different magnetic responses (Sec. III).

Electronics states vary with magnetic field; therefore, there exists magnetization in a carbon toroid. It is a variation of free energy with magnetic field. The free energy is

$$F(\phi,T)=\sum_{J,L,\sigma,h}\frac{-1}{\beta}\ln\{1+\exp[-\beta E^h(J,L,\phi;\sigma)]\}.\tag{4}$$

$\beta=1/k_B T$. Magnetization is given by

$$M(\phi,T)=-\frac{c}{2r}\frac{\partial F(\phi,T)}{\partial\phi}=-\frac{c}{2r}\sum_{h,J,L,\sigma}f[E^h(J,L,\phi;\sigma)]\frac{\partial E^h(J,L,\phi;\sigma)}{\partial\phi},\tag{5}$$

where $f[E^h(J,L,\phi;\sigma)]=[e^{\beta[E^h(J,L,\phi;\sigma)-\mu(T,\phi)]}+1]^{-1}$ is the Fermi-Dirac distribution function. The chemical potential

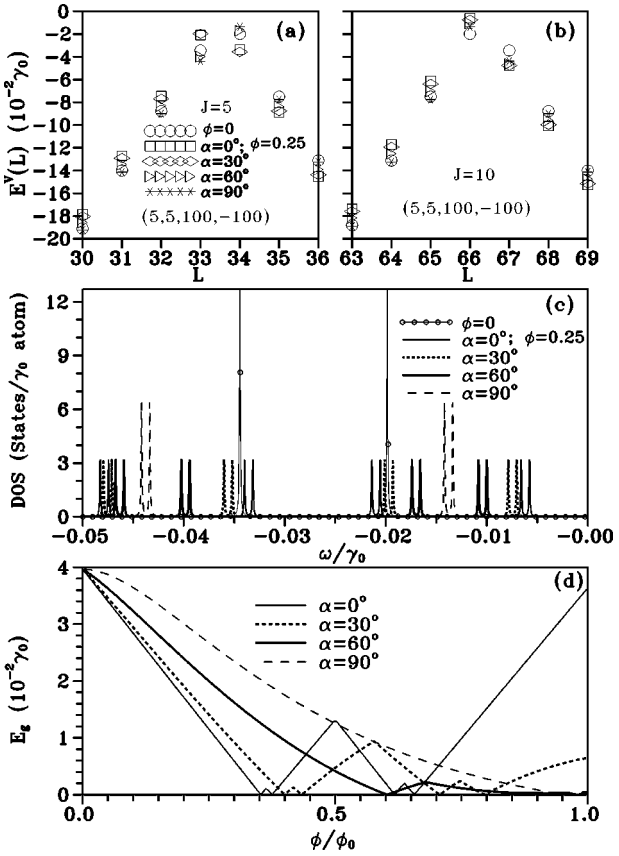

FIG. 1. The low energy electronic properties of the (5, 5, 100, −100) toroid at $\phi=0$, $\phi=0.25\ \phi_0$, and different α's. State energies of $J=5$ and $J=10$, without the Zeeman splitting, are shown in (a) and (b). For simplicity, the Zeeman splitting is neglected. Density of states and energy gap in the presence of the Zeeman splitting are shown in (c) and (d), respectively.

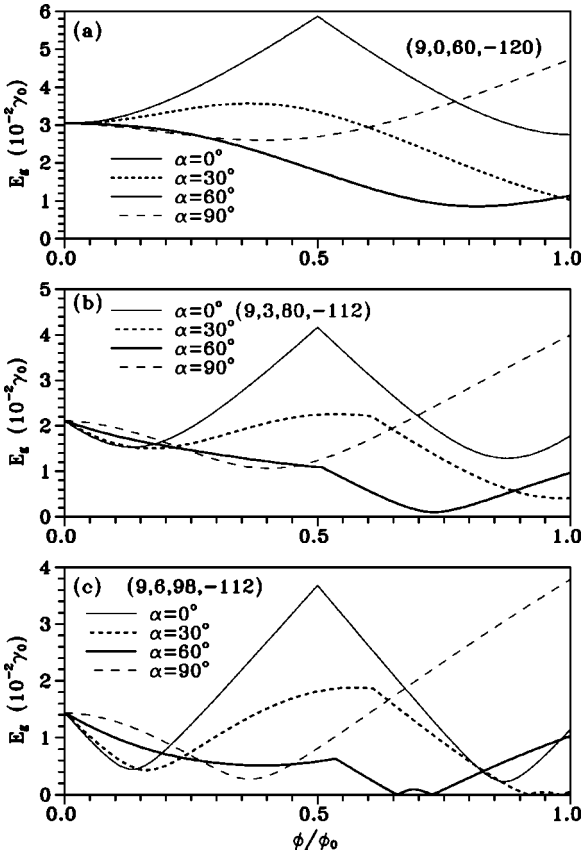

FIG. 2. The magnetic-flux-dependent energy gap is shown at different field directions for (a) the (9, 0, 60, −120) toroid, (b) the (9, 3, 80, −112) toroid, and (c) the (9, 6, 98, −112) toroid.

$\mu(T,\phi)$ is equal to zero for any T and ϕ, since the occupied states are symmetric to the unoccupied states about the Fermi level.

III. MAGNETOELECTRONIC STATES AND MAGNETIZATION

A (5,5,100,−100) armchair carbon toroid is chosen for a model study. It has many discrete electronic states as a result of the periodical boundary conditions. The occupied low energy states are shown in Figs. 1(a) and 1(b). They own fourfold degeneracy in the absence of ϕ, i.e., $E^v(J,L;\sigma)=E^v(2m-J,p-L;\sigma)$. The $(J_a=5,L_a=34)$ and $(J_a=10,L_a=66)$ states have the lowest energy. (J_a,L_a) represents the state nearest to $E_F=0$. $2|E^v(J_a,L_a)|$ is energy gap at $\phi=0$. The fourfold degeneracy is changed into the double degeneracy in the presence $\mathbf{B}_\parallel$, if the Zeeman effect is neglected. That the effects of $\mathbf{B}_\parallel$ on L and $p-L$ are different is responsible for the destruction of the fourfold degeneracy. Energy spacing between two states is also altered by ϕ. When the magnetic field deviates from the toroid axis, $\mathbf{B}_\perp$ induces the coupling of different L's in addition to the shift of L from $\mathbf{B}_\parallel$. Each wave function is the superposition of those of different L's. It is assumed to be characterized by a specific L with the maximum probability. The coupling of L's is strong for large ϕ and α. It would affect state degeneracy and energy spacing. The fourfold degeneracy is recovered at $\alpha=90°$ because of the vanishing shift of L. At $\phi>\phi_0$, the principal quantization number might be $L\pm1$ or others.

Density of states, with the Zeeman splitting, is shown in Fig. 1(c). It is symmetric about $\omega=0$. DOS exhibits a lot of delta-function-like peaks, owing to the zero-dimensional discrete states. The height of peak corresponds to the state degeneracy. They are reduced by the magnetic field except at $\alpha=90°$ and the Zeeman effect. When there are no peaks at $E_F=0$, it exists an energy gap between the HOS and the LUS. The magnetic-flux-dependent energy gap, as shown in Fig. 1(d), could change from a finite value to zero. The SMT's happen at ϕ_a's, where E_g is vanishing. The HOS and the LUS, respectivley, become unoccupied and occupied at ϕ_a's, so they would make outstanding contributions to magnetization. At large α, the dependence of E_g on ϕ is weaker. The coupling of L's is less efficient in changing energy gap, as compared with the shift of L's. It is relatively difficult to induce the SMT's. For example, there are no SMT's at $\alpha=90°$ in the absence of the Zeeman splitting. However, the Zeeman effect could induce the SMT's, or make the SMT's occur more frequently.

The cause of energy gap is discussed in detail. A two-dimensional graphite sheet is a gapless semiconductor with

the Fermi momentum k_F. The electronic states of a SCN are derived from its states according to the transverse periodical boundary condition. A SCN would exhibit the metallic behavior, when it could sample the k_F state. SCN's are, respectively, metals and large-gap semiconductors for $2m+n=3I$ and others (type III). Energy gaps of the latter are inversely proportional to the nanotube diameter (or the toroid height $2r$). The former in the presence of the curvature effect are further divided into the metallic armchair nanotubes (type I) and the narrow-gap nonarmchair nanotubes [type II; e.g., the (9,0), (9,3); (9,6) nanotubes]. Also noticed that the curvature effect leads to the shift of the Fermi momentum. The type II nanotubes have energy gaps E_g's $\propto \cos(3\theta)/(2r)^2$.[37] The chiral angles are, respectively, $\theta=0°$ and $-30°$ for zigzag and armchair nanotubes. E_g's are smaller for those nanotubes near armchair configuration.

Similarly, a carbon toroid samples the π-electron states of a SCN, which satisfies the longitudinal periodical boundary condition. Most of armchair carbon tori have E_g's $\propto 1/R$. They could not sample the k_F state, mainly owing to the curvature effect and the longitudinal periodical boundary condition. Armchair carbon tori would become gapless by the variation of the parallel magnetic field [the continuous change of L in the longitudinal periodical boundary condition; Fig. 1(d)]. As to nonarmchair carbon tori, their energy gaps are enhanced by the longitudinal periodical boundary condition. $\mathbf{B}_{\|}$ could not make them exhibit the gapless behavior, as shown in Fig. 2. Although the field direction could alter the dependence of E_g on ϕ, the SMT's are absent. The Zeeman splitting could effectively reduce energy gap and thus causes SMT's in carbon tori with larger chiral angles [e.g., the (9, 6, 98, −112) toroid in Fig. 2(c)]. In short, energy gaps of carbon tori are mainly determined by the curvature effect (or the change of the nearest-neighbor interactions), the two periodical boundary conditions (the height, the chirality, and the radius), the direction and the magnitude of the magnetic field, and the Zeeman splitting. Carbon tori close to armchair configuration could exhibit the SMT's.

The magnetic-flux-dependent magnetization is shown in Fig. 3(a). At $\alpha=0°$, it depends on ϕ linearly and exhibits two pairs of special jump structures (or four jump structures) within ϕ_0. The heights of the two jumps in each pair are equal since the contributions from the two different spin states are the same. The discontinuous structures are located at ϕ_a's, where the SMT's occur. They should be associated with the drastic changes in the electron occupation number. At the neighborhood of $\phi_a=0.353\ \phi_0$, the spin-down π^* state (the spin-up π state) of $(J_a=10, L_a=66)$ changes from the unoccupied (occupied) state into the occupied (unoccupied) state. The π^* and π states make the opposite contributions to M, so they both induce a special jump. A similar jump is obtained at $\phi_a=0.375\ \phi_0$; that is, it comes from the spin-up π^* state and the spin-down π state of $(J_a=10, L_a=66)$. Another pair of jump structures at $\phi>0.5\ \phi_0$ is due to the $(J_a=5, L_a=33)$ states.

The direction of the magnetic field has certain important effects on magnetization. The SMT's happen less frequently in the increasing of α, and so do the special jump structures. Also noticed that such structures exhibit in the pair form at any α. The height of jump is significantly reduced. That the shift of L becomes small accounts for this result. The ϕ-dependence of M changes from linearity into nonlinearity. The magnitude of magnetization grows for the sufficiently

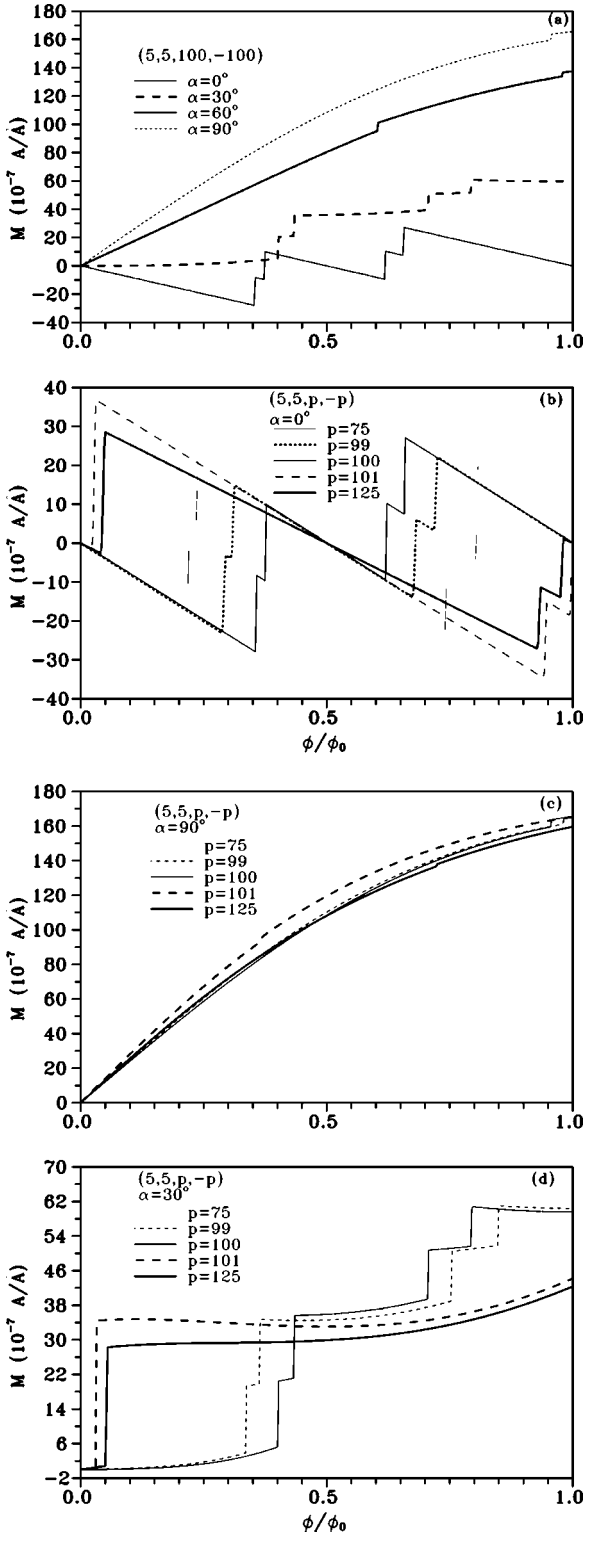

FIG. 3. The magnetic-flux-dependent magnetization is calculated for (a) the (5, 5, 100, −100) toroid at different α's, and for the (5, 5, p, $-p$) tori of different radii at (b) $\alpha=0°$, (c) $\alpha=90°$, and (d) $\alpha=30°$.

large magnetic flux ($\phi > 0.75\ \phi_0$). M might be positive or negative at $\phi \to 0$, which is dominated by the field direction. $M<0$ and $M>0$, respectively, occur at $\alpha<30°$ and $\alpha>30°$. Diamagnetism would be changed into paramagnetism as the magnetic field gradually deviates from the symmetry axis.

Magnetization is strongly affected by radius, as shown in Fig. 3(b) at $\alpha=0°$. The larger the toroid, the weaker the ϕ-dependence of M. The height of jump structure linearly decreases with increasing radius, since the velocity of the L_a state is inversely proportional to R. When the radius is sufficiently large ($p>101$), the first pair of special jump structures might become a single jump. The negligible Zeeman effect is the main reason. However, radius does not thoroughly alter magnetism at $\phi \to 0$. That is to say, most of armchair carbon tori are diamagnetic except for few systems with zero energy gap at $\phi=0$. On the other hand, at $\alpha=90°$, all armchair carbon tori exhibit paramagnetism [Fig. 3(c)]. The jump structures almost vanish. The ϕ-dependent M is not sensitive to radius at $\alpha=90°$. According to the $\alpha=0°$ and 90° cases, it seems to exist a critical angle (α_c) in determining magnetism. When armchair carbon tori have the sufficiently large radii ($p>75$), they are paramagnetic at $\alpha=30°$ [Fig. 3(d)]. Moreover, the (5, 5, 75, −75) toroid would change from diamagnetism to paramagnetism for α somewhat larger than 30°. It is deduced that the critical angle is $\alpha_c \simeq 30°$.

The chiral angle plays an important role on magnetization. All zigzag carbon tori are paramagnetic for any field direction, e.g., the (9, 0, 60, −120) toroid in Fig. 4(a). The paramagnetic response becomes strong in the increasing of α. The drastic changes due to the SMT's are absent. Similar results could also be found in the chiral carbon tori with smaller chiral angles, e.g., the (9, 3, 8, −112) toroid in Fig. 4(b). But on the other hand, the chiral carbon tori near armchair configuration exhibit the diamagnetic response for $\alpha<30°$, e.g., the (9, 6, 98, −112) toroid in Fig. 4(c). The critical angle $\alpha_c \simeq 30°$ is also present in such carbon tori. There are special jump structures in M.

When temperature increases from zero, electrons could also occupy the π^* states with $E>0$. At $\alpha=0°$, the magnetization due to the π^* electrons is opposite to that of the π states. Their competition would lead to the change from jump structures to peak structures, and the reduction in magnitude of magnetization [Fig. 5(a)]. It is difficult to observe peak structures at higher temperature ($T>300$ K). The temperature effects quickly decline as α grows. Magnetization hardly depends on temperature at $\alpha=90°$ [Fig. 5(b)].

Armchair carbon tori constrast sharply with armchair carbon nanotubes in magnetoelectronic structures and magnetization. The latter exhibit the SMT at $\phi=0$ for $\alpha \neq 90°$, and they remain metallic during the variation of ϕ for $\alpha=90°$ [Fig. 1(b) in Ref. 34]. They are, respectively, paramagnetic and diamagnetic in the presence of $\mathbf{B}_\parallel$ and $\mathbf{B}_\perp$ (Fig. 2 in Ref. 28). Moreover, they do not exhibit jump structures in magnetization. The opposites are true for the former [Figs. 1(d) and 2]. The critical angle in determining magnetism is about 30°. Whether α_c exists in armchair or nonarmchair carbon nanotubes deserves a closer examination. In addition, zigzag carbon tori and nanotubes, respectively, exhibit the paramagnetic and diamagnetic responses for $\mathbf{B}_\perp$. Such important differences clearly illustrates that both zero-dimensional carbon tori and one-dimensional carbon nanotubes are worthy of the detailed studies in magnetoelectronic properties.

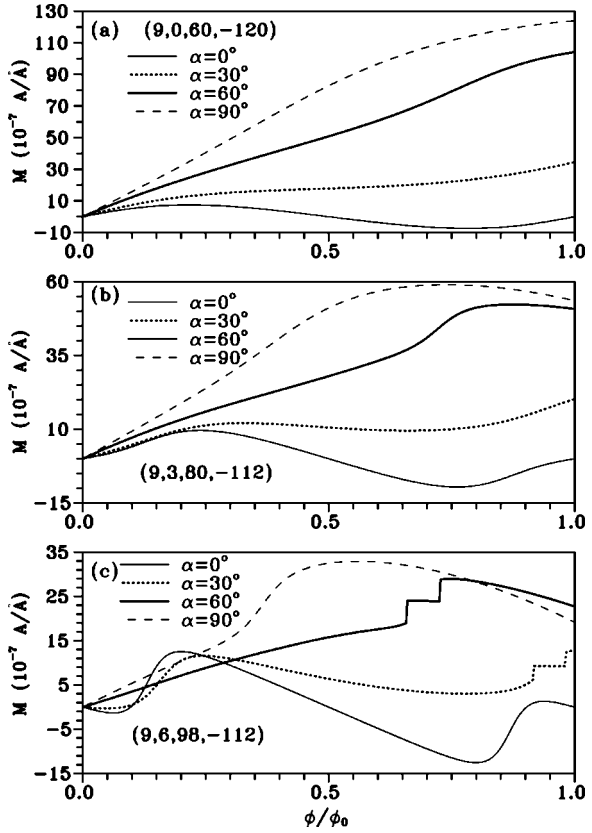

FIG. 4. Same plot as Fig. 3(a), but shown for (a) the (9, 0, 60, −120) toroid, (b) the (9, 3, 80, −112) toroid, and (c) the (9, 6, 98, −112) toroid.

Finally, the calculated magnetoelectronic properties in the presence of $\mathbf{B}_\parallel$ are compared with those in Refs. 16 and 17. The present results are different from (similar to) those obtained by the simplest zone-folding approach without the curvature effect in Ref. 16 (the Slater Koster approach in Ref. 17). The former predict that most of armchair tori and all $(3m,0,p,-2p)$ zigag tori have a small energy gap at vanishing magnetic flux. They are, respectively, diamagnetic and paramagnetic at very small flux [Figs. 2(b) and 3(a) and Fig. 9 in Ref. 17]. The paramagnetic response does not belong to the giant magnetic response. On the other hand, the latter show that all $(3m,0,p,-2p)$ zigzag tori and the third of armchair tori are metallic, and the other armchair tori are semiconducting. The metallic and semiconducting tori, respectively, exhibit the giant paramagnetic response and the diamagnetic response. These differences mainly come from the curvature effect, as discussed earlier in the cause of energy gap. It might be difficult to observe the colossal paramagnetic response[16] in carbon tori.

IV. CONCLUDING REMARKS

In this work, we have studied magnetoelectronic properties of armchair carbon tori for any magnetic field. Electronic

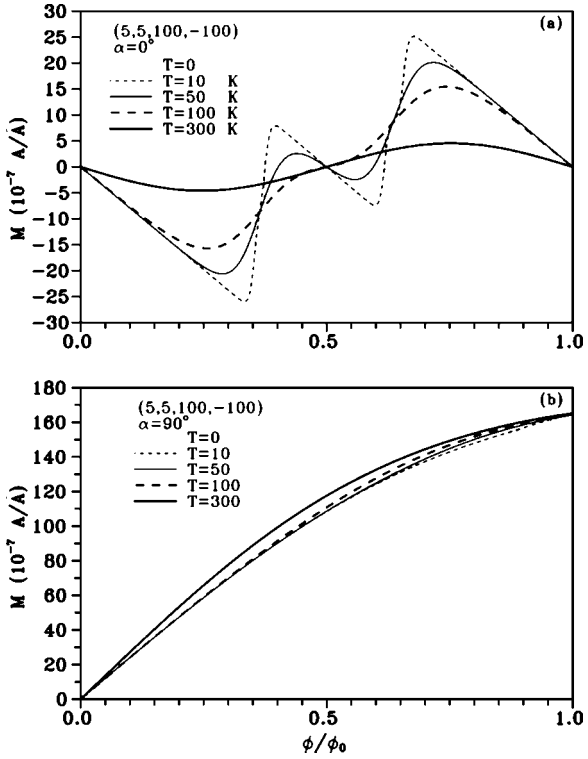

FIG. 5. The magnetic-flux-dependent magnetization of the (5, 5, 100, −100) toroid is calculated at different temperatures, and (a) $\alpha=0°$; (b) $\alpha=90°$.

states within the tight-binding model are dominated by the magnitude and the direction of the magnetic field. **B** causes the destruction of state degeneracy, the change of energy spacing, the metal-semiconductor transition, and the alternation of the quantization of wavefunction. There are more SMT's when **B** is oriented closer to the symmetry axis. SMT's further lead to the special jump structures in magnetization at $T=0$. Magnetization is dependent on the radius, the temperature, the field direction, and the chirality. The dependence on $R(T)$ is strong for $\mathbf{B}_{\|}$, while it is weak for $\mathbf{B}_{\perp}$. Most of armchair carbon tori, respectively, exhibit paramagnetism and diamagnetism for $\alpha>30°$ and $\alpha<30°$. The critical angle $\alpha_c\simeq 30°$ also exists in chiral carbon tori near armchair configuration. However, the other carbon tori with smaller chiral angles are paramagnetic for any field direction. The main differences between armchair carbon tori and armchair carbon nanotubes (or zigzag carbon tori) include the SMT's, the magnetism, and the special structures in magnetization.

ACKNOWLEDGMENTS

This work was supported in part by the National Science Council of Taiwan, the Republic of China under Grant Nos. NSC 92-2112-M-145-001, 92-2112-M-006-014, and 92-2112-M-165-001.

[1] S. Iijima, Nature (London) **354**, 56 (1991).
[2] J. Liu, H. Dai, J. H. Hafner, D. T. Colbert, R. E. Smalley, S. J. Tans, and C. Dekker, Nature (London) **385**, 780 (1997).
[3] For the details of geometric structures see M. F. Lin, R. B. Chen, and F. L. Shyu, Solid State Commun. **107**, 227 (1998).
[4] B. I. Dunlap, Phys. Rev. B **46**, 1933 (1992).
[5] S. Itoh, S. Ihara, and J. I. Kitakami, Phys. Rev. B **47**, 1703 (1993).
[6] D. H. Oh, J. M. Park, and K. S. Kim, Phys. Rev. B **62**, 1600 (2000).
[7] S. A. Bovin, L. F. Chibotaru, and A. Ceulemans, J. Mol. Catal. A: Chem. **166**, 47 (2001).
[8] V. Meunier, Ph. Lambin, and A. A. Lucas, Phys. Rev. B **57**, 14886 (1998).
[9] A. Ceulemans, L. F. Chibotaru, and S. A. Bovin, J. Chem. Phys. **112**, 4271 (2000).
[10] A. Latge, C. G. Rocha, L. A. L. Wanderley, M. Pacheco, P. Orellana, and Z. Barticevic, Phys. Rev. B **67**, 155413 (2003).
[11] M. F. Lin and D. S. Chuu, J. Phys. Soc. Jpn. **67**, 259 (1998).
[12] M. F. Lin and D. S. Chuu, Phys. Rev. B **57**, 6731 (1998).
[13] R. C. Haddon, Nature (London) **388**, 31 (1997).
[14] M. F. Lin, J. Phys. Soc. Jpn. **67**, 1094 (1998).
[15] A. A. Odintsov, W. Smit, and H. Yoshioka, Europhys. Lett. **45**, 598 (1999).
[16] L. Liu, G. Y. Guo, C. S. Jayanthi, and S. Y. Wu, Phys. Rev. Lett. **88**, 217206 (2002).
[17] S. Latil, S. Roche, and A. Rubio, Phys. Rev. B **67**, 165420 (2003).
[18] S. Sasaki, Phys. Rev. B **65**, 155429 (2002).
[19] M. F. Lin, J. Phys. Soc. Jpn. **68**, 1102 (1999).
[20] M. F. Lin, J. Phys. Soc. Jpn. **69**, 3429 (2000).
[21] M. F. Lin, Phys. Rev. B **58**, 3629 (1998).
[22] M. F. Lin, J. Phys. Soc. Jpn. **62**, 2218 (1998).
[23] M. F. Lin, J. Phys. Soc. Jpn. **68**, 3585 (1999).
[24] M. F. Lin, J. Phys. Soc. Jpn. **68**, 3744 (1999).
[25] H. R. Shea, R. Martel, and Ph. Avouris, Phys. Rev. Lett. **84**, 4441 (2000).
[26] H. Ajiki and T. Ando, J. Phys. Soc. Jpn. **62**, 1255 (1993).
[27] H. Ajiki and T. Ando, J. Phys. Soc. Jpn. **62**, 2470 (1993).
[28] H. Ajiki and T. Ando, J. Phys. Soc. Jpn. **64**, 4382 (1995).
[29] H. Ajiki and T. Ando, J. Phys. Soc. Jpn. **64**, 260 (1995).
[30] H. Ajiki and T. Ando, J. Phys. Soc. Jpn. **65**, 505 (1996).
[31] R. Saito, G. Dresselhaus, and M. S. Dresselhaus, Phys. Rev. B **50**, 14698 (1994); **53**, 10408(E) (1996).
[32] S. Roche, G. Dresselhaus, M. S. Dresselhaus, and R. Saito, Phys. Rev. B **62**, 16092 (2000).
[33] F. L. Shyu, C. P. Chang, R. B. Chen, and M. F. Lin, J. Phys. Soc. Jpn. **72**, 454 (2003).
[34] F. L. Shyu, C. P. Chang, R. B. Chen, C. W. Chiu, and M. F. Lin, Phys. Rev. B **67**, 045405 (2003).
[35] C. W. Chiu, C. P. Chang, F. L. Shyu, R. B. Chen, and M. F. Lin, Phys. Rev. B **67**, 165421 (2003).
[36] M. F. Lin and K. W.-K. Shung, Phys. Rev. B **52**, 8423 (1995).
[37] C. L. Kane and E. J. Mele, Phys. Rev. Lett. **78**, 1932 (1997).
[38] J. M. Luttinger, Phys. Rev. **84**, 814 (1951).